Journal of ELECTRONIC MATERIALS, Vol. 35, No. 11, 2006 *Regular Issue Paper*

Effect of Settlement on Dense Slurry Flow in a Horizontal Channel

R. YANG,[1] D.C. SUN,[2,3] and SEUNGBAE PARK[2]

1.—Spirent Communications, Inc. 15200 Omega Drive Rockville, MD 20850. 2.—Department of Mechanical Engineering State University of New York at Binghamton Binghamton, NY 13902-6000. 3.—E-mail: dcsun@binghampton.edu

A shear viscosity model for the underfill flow is proposed based on slug flow, which is appropriate in the case of neutrally buoyant particles. However, the filling particles used in practice are often heavier than the liquid carriers. The effect of non-neutrally buoyant particles is investigated in this work. The flow of dense slurry in which the filling particles are heavier than the liquid carrier is analyzed by considering the particle-particle and particle-wall interactions, which are derived from fluid film lubrication theory. The effect of settlement causes the flow behavior to depart from that of slug flow. Nevertheless, steady flow is still found possible, and, for a few representative packing patterns considered, somewhat modified flow patterns exist.

Key words: Underfill encapsulant, underfill flow, effect of settlement

INTRODUCTION

This work was motivated by the need to understand the flow behavior of dense slurry in a narrow gap. The intended application is underfill encapsulation of electronics packaging, especially in flip chip packages and chip on board (COB) applications. The purpose of encapsulation is to protect the solder interconnects linking the silicon chip and the substrate from damage arising from the mismatch of the coefficients of thermal expansion (CTE) of the two materials. The underfill encapsulant is dense slurry consisting of a liquid carrier filled with particles (or fillers) in high volume fraction. Flow of the underfill into the gap between the chip and the substrate is driven by capillary action governed by the small height of the gap. Two manufacturing concerns arise regarding the underfill flow. One is the slow flow speed and curing time that make the filling process inefficient. The other is the formation of voids around the solder interconnects that reduces the reliability of the package. Various methods have been tried and proposed to improve on these two aspects, such as filling at elevated temperature, filling under pressure or vacuum, multiple-boundary dispensing, or the opening of dispensing passages at critical spots. Clearly, the foundation of all these remedies is understanding the flow behavior of dense slurry in geometries relevant to the package.

A key material parameter that governs the flow behavior of dense slurry is its effective viscosity. In Ref. 1, a model of the effective viscosity is advanced, where the flow behavior is considered to be governed by the interactions between neighboring particles and between particles and channel walls, and these interactions are realized through thin liquid films trapped between the solid surfaces. Fluid film lubrication theory is used to obtain the formulas of these interactions, which are then applied to the flow, between two horizontal parallel walls, of slurry densely packed with neutrally buoyant particles. When the effect of settlement is not present, the particles cluster in the middle of the channel due to the stronger particle-wall interaction. A slug flow is therefore envisioned, where the particles are so tightly packed that no gap is left between the closest neighbors. The filler particles have no relative motions with respect to each other, and move along the channel as a slug. Three packing patterns were considered for the particles in the slug, namely the rectangular cubic (rc), body-centered cubic (bcc), and face-centered cubic (fcc). Closed-form formulas for the effective viscosity of the flow are obtained.

In practice, however, the filler particles in the encapsulants are often heavier than the liquid carriers. During flow, the particles tend to settle toward the bottom wall and, because of unequal drags from the top and bottom sides, also tend to rotate. Then the particles would have relative motions with respect to each other, and the slug flow model may not represent the underfill flow well. This paper is devoted to the study of the departure from slug flow due to the settlement effect. Specifically, the issues to be resolved are whether steady flow is still possible,

(Received February 22, 2006; accepted June 22, 2006)

and whether some modified patterns would result for the three representative packing patterns.

TRANSIENT MOTION

Consider the transient motion of a slurry containing one layer of spheres (of radius R) between two closely spaced horizontal walls (see Fig. 1). The motion is driven by a given pressure gradient along the channel. Let the spheres initially be evenly spaced with gap s, their distances from the top and bottom walls being equal, and possess neither translational nor rotational velocities. After the motion starts, the gap s remains constant because every sphere is subjected to the same set of forces. However, due to gravity the distance with the top wall, h_t, increases and that with the bottom wall, h_b, decreases. The unequal drags from the two walls then cause the spheres to rotate. Let the position of the center of a representative sphere be (x_p, z_p), its corresponding velocity components be (u,w), the rotational velocity of the sphere be Ω, the mass of the sphere be m, and its moment of inertia be I $(= 2mR^2/5)$. It is further specified that

$$h_t + h_b = \bar{\delta}s \tag{1}$$

where the parameter $\bar{\delta}$ characterizes the particle-wall clearance relative to the particle-particle clearance. Note that the two clearances are independent of each other and must be specified in a problem, thus the introduction of a dimensionless parameter $\bar{\delta}$.

The forces acting on the sphere are shown in Fig. 2. The hydrostatic force (not shown) due to the given pressure gradient is

$$F_{pres} = \left(-\frac{dp}{dx}\right)\frac{4}{3}\pi R^3 \tag{2}$$

The forces W_{st} and W_{sb} are due to squeeze action caused by the sphere approaching either the top or the bottom wall. These forces may be written as[1]

$$W_{st} = 6\pi\mu wR\left(\frac{R}{h_t}\right)H(w) \tag{3}$$

$$W_{sb} = 6\pi\mu(-w)R\left(\frac{R}{h_b}\right)H(-w) \tag{4}$$

where H(w) is the Heavyside function defined as

$$\begin{aligned} H(w) &= 1 \quad \text{if } w > 0 \\ &= 0 \quad \text{if } w \le 0 \end{aligned} \tag{5}$$

Note that if the sphere moves away from a wall, there is no (negative) squeeze action between them. The forces W_t and W_b are due to entrainment action between the sphere and the walls and can be expressed as[1]

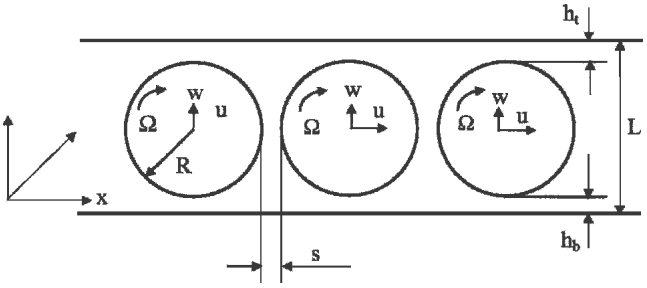

Fig. 1. Transient motion of one layer of spheres.

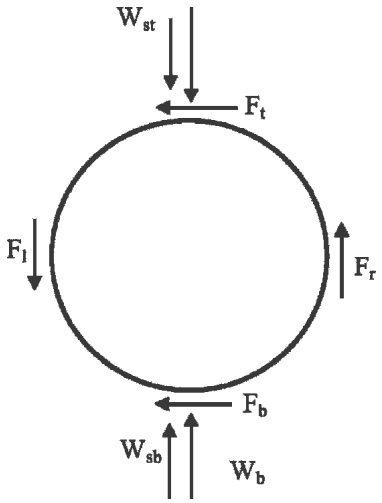

Fig. 2. Forces acting on a sphere (weight and pressure forces not shown).

$$W_t = 9.72411\left(\frac{R}{h_t}\right)^{0.51953}\mu\frac{u-\Omega R}{2}R \tag{6}$$

$$W_b = 9.72411\left(\frac{R}{h_b}\right)^{0.51953}\mu\frac{u+\Omega R}{2}R \tag{7}$$

The forces F_t and F_b are the friction forces arising from the interaction with the two walls and can be expressed as[1]

$$\begin{aligned} F_t = {} & 2\pi\mu(u+\Omega R)R\ln\left(1+\frac{R}{2h_t}\right) \\ & - 3.80525\mu\frac{u-\Omega R}{2}R\ln\left(\frac{R}{h_t}\right) \\ & + 7.95520\mu\frac{u-\Omega R}{2}R \end{aligned} \tag{8}$$

$$\begin{aligned} F_b = {} & 2\pi\mu(u-\Omega R)R\ln\left(1+\frac{R}{2h_b}\right) \\ & - 3.80525\mu\frac{u+\Omega R}{2}R\ln\left(\frac{R}{h_b}\right) \\ & + 7.95520\mu\frac{u+\Omega R}{2}R \end{aligned} \tag{9}$$

There is no entrainment action between the neighboring spheres because the two surfaces move

in opposite directions. Therefore, the entrainment velocity U is zero. Hence, there are only friction forces acting between them. These friction forces are[1]

$$F_l = F_r = 2\pi\mu\Omega R^2 \ln\left(1 + \frac{R}{4s}\right) \tag{10}$$

Note that the reduced radius for two equal-sized spheres is R/2.[1]

The equations of motion for the sphere may therefore be written as:

$$m\frac{du}{dt} = F_{pres} - F_t - F_b \tag{11}$$

$$m\frac{d^2z_p}{dt^2} = -(\rho_s - \rho_l)g\frac{4}{3}\pi R^3 - W_t - W_{st} + W_b + W_{sb} \tag{12}$$

$$I\frac{d\Omega}{dt} = F_b R - F_t R - F_l R - F_r R \tag{13}$$

where g is the gravitational constant, and ρ_s and ρ_l are the densities of the sphere and liquid, respectively.

The variables and equations are normalized before solutions are sought. Because the flow is driven by a given pressure gradient, the latter is used as the main reference quantity for normalization. The dimensionless variables are defined as:

$$\bar{z}_p = \frac{z_p}{s} \quad \bar{h}_t = \frac{h_t}{s} \quad \bar{h}_b = \frac{h_b}{s} \quad \bar{t} = t\frac{\left(-\frac{dp}{dx}\right)R}{\mu}$$

$$\bar{u} = \frac{\mu u}{R^2(-dp/dx)} \quad \bar{w} = \frac{\mu w}{R^2\left(-\frac{dp}{dx}\right)} \quad \bar{\Omega} = \frac{\mu\Omega}{R(-dp/dx)}$$

$$\bar{W} = \frac{W}{R^3\left(-\frac{dp}{dx}\right)} \quad \bar{F} = \frac{F}{R^3\left(-\frac{dp}{dx}\right)} \tag{14}$$

After normalization, four dimensionless parameters appear in the formulation. They are the tightness parameter $\bar{\varepsilon} \equiv \frac{s}{R}$, the particle-wall clearance parameter $\bar{\delta}$, the inertia parameter $\bar{m} \equiv \frac{m}{\mu^2}\left(-\frac{dp}{dx}\right)$, and the gravity parameter $\bar{\beta} \equiv \frac{(\bar{\alpha} - 1)\rho_l g}{-dp/dx}$ where $\bar{\alpha}$ is the density ratio ρ_s/ρ_l.

The material properties and dimensions used in the calculation are those used in a laboratory experimental study of the underfill flow and are as follows:

$$\rho_l = 0.83 \cdot 10^3 \text{ kg/m}^3$$

$$\rho_s = 2.5 \cdot 10^3 \text{ kg/m}^3$$

$$\mu = 0.019 \text{ Ns/m}^2$$

$$\sigma \text{ (surface tension of liquid carrier)} = 30 \cdot 10^{-3} \text{N/m}$$

$$R = 25 \cdot 10^{-6} \text{ m}$$

$$L \text{ (channel height)} = 100 \times 10^{-6} \text{ m}$$

By using these σ and L values, the pressure jump across the meniscus of the flow front may be estimated as:

$$\Delta p = \frac{2\sigma}{L} = 600 \text{ N/m}^2$$

For a channel length of about 40 mm, a representative pressure gradient value is:

$$-\frac{dp}{dx} = 15200 \text{ N/m}^3$$

Based on the above values, it is found that

$$\bar{\alpha} = 3.012, \quad \bar{\beta} = 1.077, \quad \bar{m} = 6.89 \times 10^{-3}$$

The system of Eqs. (11–13) in dimensionless form was integrated using the Runge-Kutta method. The system is stiff because of the presence of small parameters $\bar{m}$ and $\bar{\varepsilon}$ in the coefficients of the highest order derivatives. The time step used had to be very small. After several trials, a time step of 5×10^{-7} was adopted. The calculation was carried out for a total of 4×10^7 time steps. Figure 3 presents the results of $\bar{u}$, $\bar{w}$, $\bar{\Omega}$, and $\bar{z}_p$ for $\bar{\varepsilon} = 0.001$ and $\bar{\delta} = 2$.

It is seen that the velocity components jump from their initial zero values to high magnitudes almost instantly (within 1000 time steps); then $\bar{u}$ readjusts itself very gently while $\bar{w}$ rapidly decays to zero. The rotational velocity $\bar{\Omega}$ and the particle's vertical position both settle to their final values exponentially. At $\bar{t} = 20$, (i.e., 1 sec after the flow starts), the values obtained are:

$$\bar{u} = 0.069667$$

$$\bar{w} = -6.5 \times 10^{-7}$$

$$\bar{\Omega} = 0.0011397$$

$$\bar{z}_p = -0.30234 \text{ (corresponding to } \bar{h}_t = 1.30234, \; \bar{h}_b = 0.69766)$$

These values are in agreement with the steady state values obtained by solving Eqs. (11–13) with the time-derivatives and w set to zero. The dimensional velocity is calculated to be $u = 34.833 \times 10^{-6}$ m/s. Using this value as a guide, it takes about 19 min. for the slurry to flow through a channel 40 mm long. In comparison, the transient period leading to the steady state is indeed very short. Therefore, in the following only the steady-state flow will be of concern.

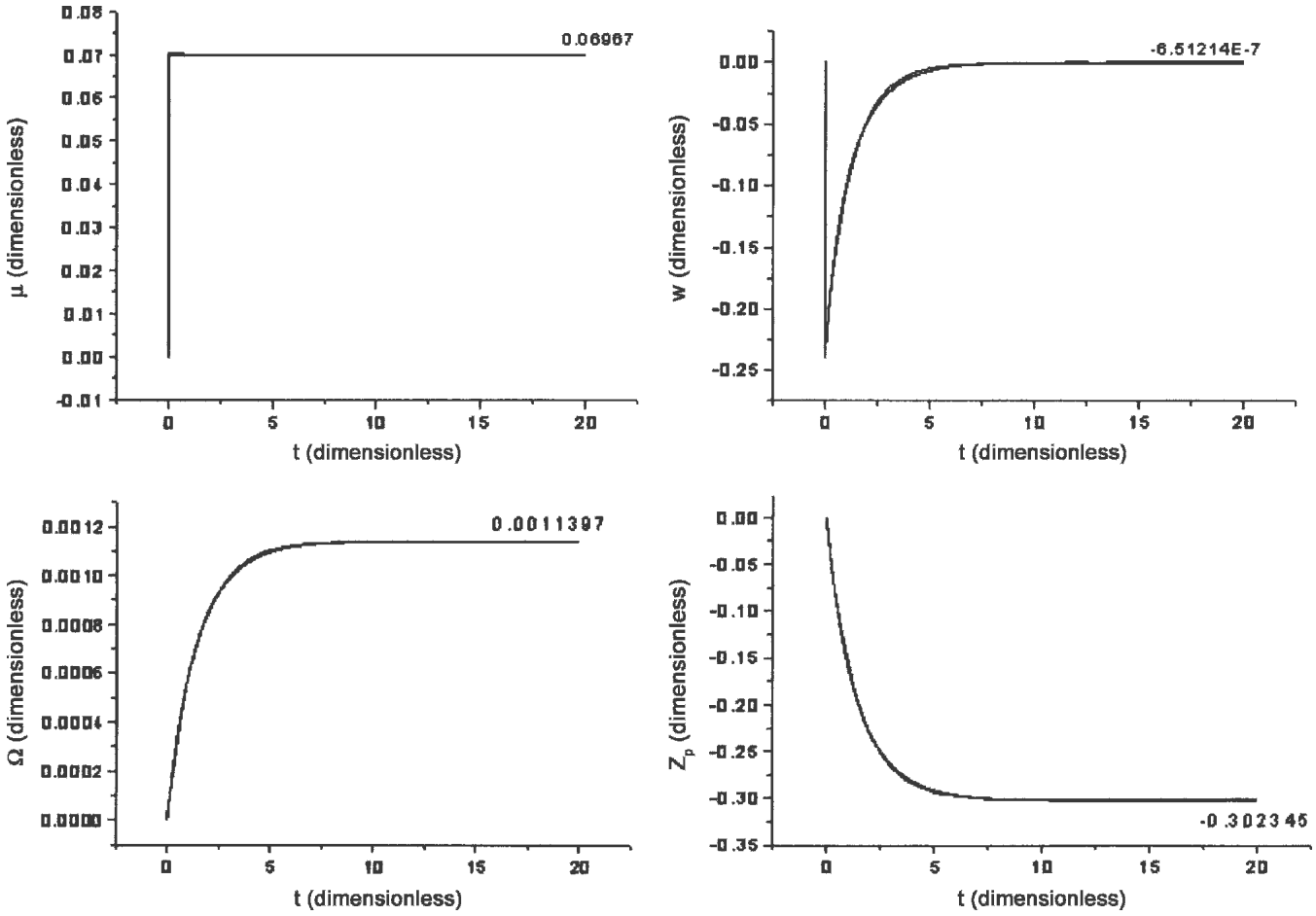

Fig. 3. Transient solution for one layer of spheres flowing in a closely spaced channel ($\bar{\varepsilon} = 0.001$, $\bar{\delta} = 2$, $\bar{\beta} = 1.077$, $\bar{m} = 6.89 \times 10^{-3}$).

STEADY MOTION

Consider the three packing patterns of particles,[1] namely the rc, bcc, and fcc packing patterns. Because of gravity, particles will settle, develop relative motions with respect to each other, and arrange themselves differently than they were in the original patterns. These cases are treated separately below.

Rectangular Cubic Packing Pattern

Consider that the channel contains one rc cell in the z-direction. After steady motion is established, the equilibrium configuration may be as sketched in Fig. 4. The spheres shown are all located in the (x, z) plane. To preserve a continuous pattern, the distance between neighboring spheres in the same layer (both the top and the bottom) must be a constant s. However, the two layers are not aligned, and two distances, b and d, are used to describe the distorted pattern. A geometrical relation may be written as:

$$b + 2R + h_t + h_b = L \tag{15}$$

To characterize the particle-wall clearance relative to the particle-particle clearance, a parameter $\bar{\delta}$ is introduced such that

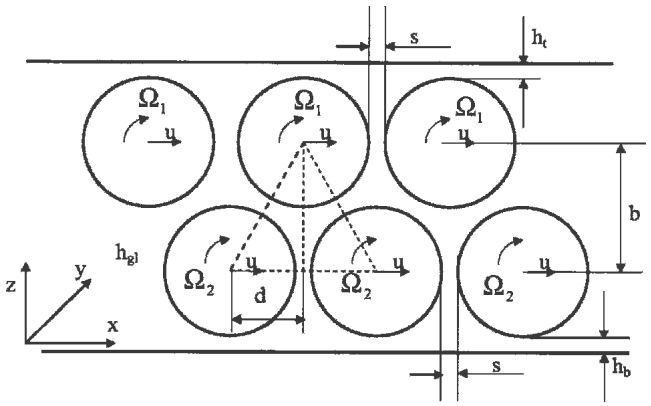

Fig. 4. Steady-state flow of one cell of rectangular cubic packing.

$$L - 4R = \bar{\delta}s \tag{16}$$

Combining Eqs. (15) and (16), one obtains:

$$b - 2R + h_t + h_b = \bar{\delta}s \tag{17}$$

Let all the spheres translate with the same velocity u, the spheres in the top layer rotate with angular velocity Ω_1, those in the bottom layer rotate with Ω_2 (directions of Ω_1 and Ω_2 as shown). Then, there are seven unknowns to be determined, namely, u, Ω_1, Ω_2, b, d, h_t, and h_b.

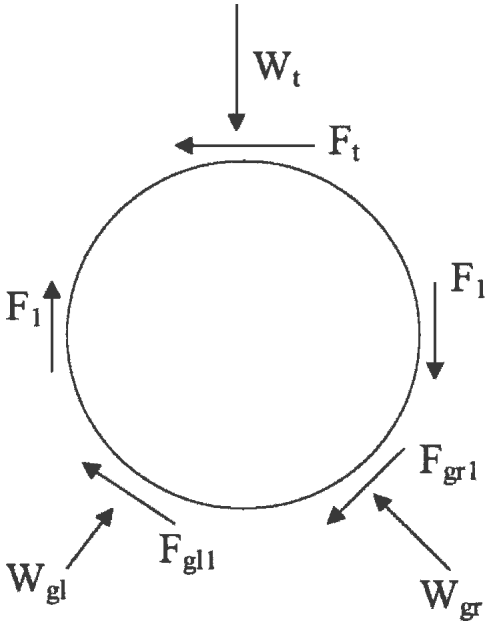

Fig. 5. Forces acting on a top layer sphere (weight and pressure forces not shown).

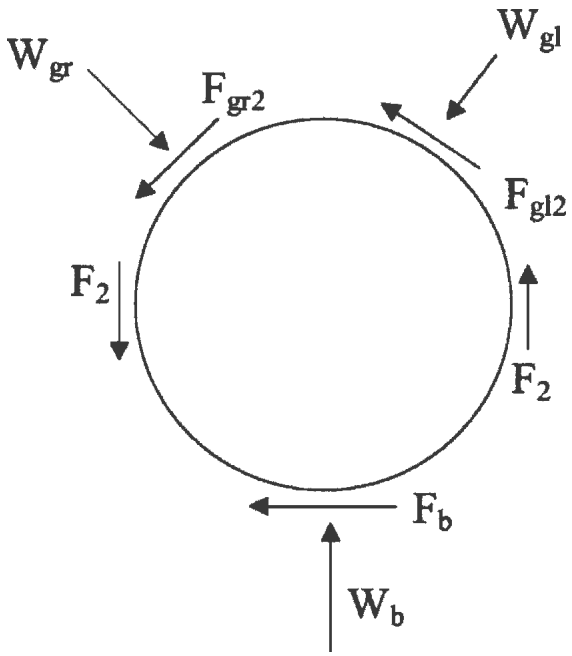

Fig. 6. Forces acting on a bottom layer sphere (weight and pressure forces not shown).

The forces acting on a representative top layer sphere are shown in Fig. 5, and those on a representative bottom layer sphere in Fig. 6. These forces can be obtained, based on the formulas given in Ref. 1 in the same way as in the Transient Motion section. Note that in steady flow, no squeeze forces are present. For each sphere, three equilibrium equations may be written (one for the forces in the x-direction, one for the forces in the z-direction, and one for the moments about the y-axis). Along with Eq. 17, there are altogether seven equations.

The parameters in the problem are $\bar{\varepsilon}$, $\bar{\beta}$ (which includes the effect of $\bar{\alpha}$), and $\bar{\delta}$ as defined in Eq. 16. The inertia parameter $\bar{m}$ is no longer present because a steady-state problem is being dealt with.

MATHCAD[2] was used to solve the equations. It was found that employing proper initial values greatly helped the convergence of the built-in iteration processes. The converged solution was then verified by checking the residues of the equations. Table I lists the solutions for four cases, where all the variables are normalized as in the Transient Motion section, with the additional variables b and d normalized by particle radius R.

For example, in the case of $\bar{\varepsilon} = 0.001$ and $\bar{\delta} = 1$ (i.e., the particle radius is 1000 times the interparticle clearance s, and the channel height is one s larger than the height of two particles stacked together), it is found that all the particles translate downstream at the same dimensionless velocity (0.35309); the bottom layer spheres rotate at a dimensionless speed (0.04976) faster than that of the top layer spheres (0.03645); and the direction of rotation of the top layer spheres is opposite that shown in Fig. 4. The distance between the two layers of spheres is b = 1.73339R (in contrast to 2R in the case of slug flow), and the top layer spheres shift 1.00185R downstream relative to the bottom layer spheres. The distance of the spheres from the bottom wall (25.91791s) is of course smaller than that from the top wall (241.68718s), as a result of the gravity effect. However, both values are much larger than the interparticle clearance.

Body-Centered Cubic Packing Pattern

Consider that the channel contains one bcc cell in the z-direction. If there is no distortion of the cell, its size is

$$e = \frac{4R + 2s}{\sqrt{3}} \tag{18}$$

where s is the smallest gap between a corner sphere and the center sphere. After steady motion is established, the distorted cell may be sketched as shown in Fig. 7. The cell size in the top layer and in the bottom layer must remain the same e. However, the two layers may be misaligned in the x-direction. The center sphere is shifted in the x-direction. Furthermore, because of gravity, the distance of the center spheres from the top layer is different than that from the bottom layer. The distorted pattern may be described by distances d_1, d_2, b_1, b_2, and e. A geometrical relation may be written as

$$b_1 + b_2 + 2R + h_t + h_b = L \tag{19}$$

where L is the channel height. To characterize the particle-wall clearance to the particle-particle clearance, a parameter $\bar{\delta}$ is introduced such that

$$e + 2R + \bar{\delta}s = L \tag{20}$$

Combining Eqs. (19) and (20), one obtains:

Table I. Results in the Case of Rectangular Cubic Packing Pattern ($\alpha = 3.012$, $\beta = 1.077$)

		$\varepsilon = 0.005$	$\varepsilon = 0.001$
$\delta = 1$	u	0.36516	0.35309
	Ω_1	−0.04947	−0.03645
	Ω_2	0.06388	0.04976
	h_t	48.73614	241.68718
	h_b	5.64179	25.91791
	b	1.73311	1.73339
	d	1.00436	1.00185
$\delta = 3$	u	0.36714	0.35350
	Ω_1	−0.04949	−0.03645
	Ω_2	0.06405	0.04978
	h_t	50.62038	243.58143
	h_b	5.74642	26.01633
	b	1.73317	1.73340
	d	1.00443	1.00186

All variables in dimensionless form.

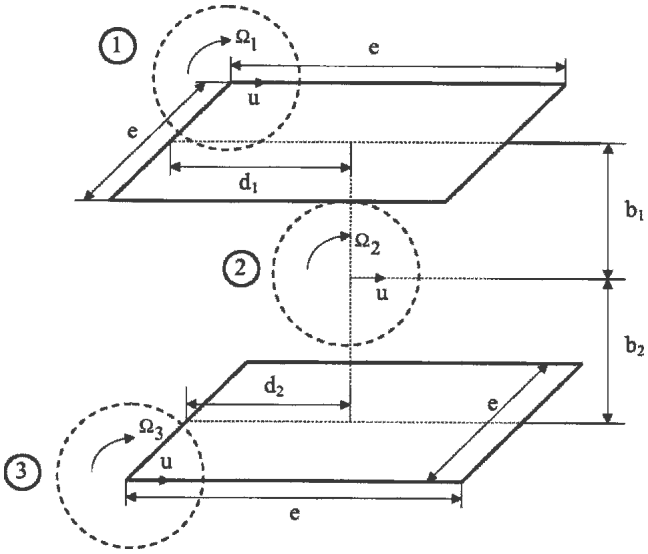

Fig. 7. Steady-state flow of one cell of bcc packing.

$$b_1 + b_2 + h_t + h_b - e = \bar{\delta}s \tag{21}$$

Let the rotational velocities of the three representative spheres 1, 2, and 3 be Ω_1, Ω_2, and Ω_3, respectively, as shown in Fig. 7, but the three spheres translate with the same velocity u. Thus, there are ten unknowns to be determined: u, Ω_1, Ω_2, Ω_3, b_1, b_2, d_1, d_2, h_t, and h_b.

The forces acting on the three representative spheres are sketched in Fig. 8. These forces can be similarly obtained by using the formulas given in Ref. 1. The work is, however, tedious because the forces acting on each sphere are not coplanar. For brevity, the derivation is not given here. The details can be found in Yang.[3] Again, one can write three equilibrium equations for each sphere. (The equilibrium of forces in the y-direction is automatically satisfied by symmetry.) Along with Eq. 21, there are altogether ten equations.

The parameters in the problem are $\bar{\varepsilon}$, $\bar{\beta}$ (which includes the effect of $\bar{\alpha}$), and $\bar{\delta}$ as defined in Eq. 20. MATHCAD[2] was used to solve the ten equations. It was even more difficult than the case of rc packing to reach convergence of the iteration processes. Solutions were obtained with careful selections of the initial values. Table II lists the solutions for four

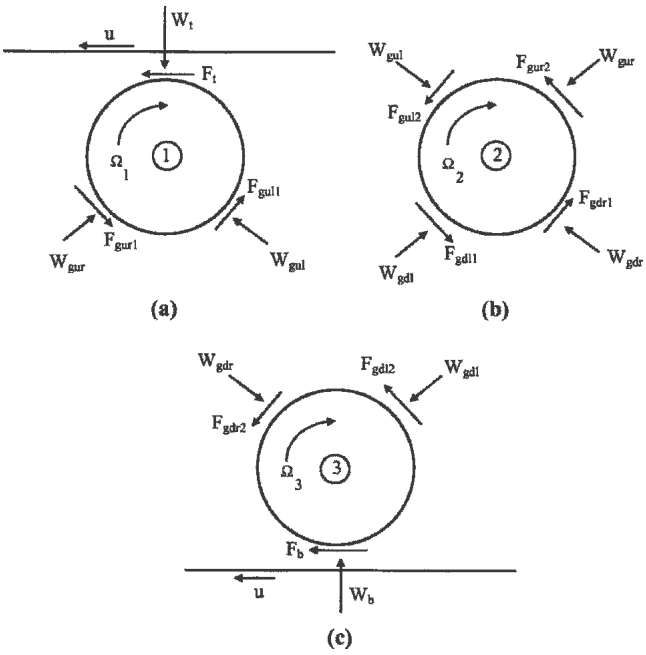

Fig. 8. Forces acting on the three representative spheres (weight and pressure forces not shown). Note that the forces on each sphere are not coplanar and not all the forces are shown.

Table II. Results in the Case of Body-Centered-Cubic Packing Pattern ($\alpha = 3.012$, $\beta = 1.077$)

		$\varepsilon = 0.005$	$\varepsilon = 0.001$
$\delta = 1$	u	0.31897	0.25040
	Ω_1	−0.00612	−0.04597
	Ω_2	−0.00366	−0.00132
	Ω_3	0.06506	0.05074
	h_t	3.34689	2.90666
	h_b	1.04519	1.46229
	b_1	1.14907	1.15359
	b_2	1.14914	1.15359
	d_1	1.15765	1.15529
	d_2	1.15768	1.15529
$\delta = 3$	u	0.33950	0.26362
	Ω_1	−0.05102	−0.04725
	Ω_2	−0.00458	−0.00168
	Ω_3	0.06962	0.05339
	h_t	4.99418	4.34307
	h_b	1.36835	1.98678
	b_1	1.14912	1.15361
	b_2	1.14925	1.15362
	d_1	1.15767	1.15529
	d_2	1.15773	1.15530

All variables in dimensionless form.

cases, where all the variables are normalized as in the Transient Motion section, with the additional variables b_1, b_2, d_1, d_2 normalized by particle radius R.

For example, in the case of $\bar{\varepsilon} = 0.001$ and $\bar{\delta} = 3$ (i.e., the particle radius is 1000 times the interparticle clearance s, and the channel height is three s larger than the cell size plus two times the radius), it is found that all the particles translate downstream at the same dimensionless velocity (0.26362); the bottom layer spheres rotate the fastest (at a dimensionless speed of 0.05339); the top layer spheres rotate with a dimensionless speed of 0.04725 opposite to the direction shown in Fig. 7; and the middle layer spheres rotate at an almost negligible speed (−0.00168). The cell size in the z-direction is reduced to $b_1 + b_2 = 2.30723$R, in contrast to the undistorted size of 2.31056R as given by Eq. 18. The shifted positions of the top and bottom layer spheres are $d_1 = 1.15529R$ and $d_2 = 1.15530R$, respectively, relative to the middle layer spheres. Compared with the undistorted position of 1.15528R, such shifts are indeed very minute. The distance of the spheres from the bottom wall ($h_b = 1.98678$s) is of course smaller than that from the top wall ($h_t = 4.34307$s) due to gravity. However, both values are still quite large compared with the interparticle clearance.

Face-Centered Cubic Packing Pattern

Consider that the channel contains one fcc cell in the z-direction. Figure 9 shows a sketch of four such cells in the undistorted configuration. Let the situation be first simplified with symmetry arguments. Consider the top layer of spheres. The center spheres B_1, B_2, D_1, D_2, and the corner sphere C_2 also form a cell (shown by the long dashed lines). Suppose that, in the steady-state flow, the center sphere B_2 in the cell $A_2A_3C_2C_3$ were closer to the line C_2C_3. Then the center sphere C_2 in the cell $B_1B_2D_1D_2$ would be farther from the line D_1D_2, which contradicts the supposition. Therefore, the center sphere of any cell must remain in the middle. This argument applies not only to the top layer, but also to the middle and bottom layers as well. Thus, to analyze the steady-state flow configuration, only three spheres, such as A_1, F_1, G_1, need to be considered, and only four distance parameters, similar to the distances d_1, d_2, b_1, b_2 in Fig. 7, need to be used to describe the distorted pattern. There are ten equations (three equilibrium equations for each sphere and one equation describing the geometric constraint) to solve for ten unknowns (one translational velocity, three rotational velocities, the clearances with the top and bottom walls, and the four distance parameters mentioned above), just like the bcc case. It is conceivable that the solution to the problem can be found, as in the bcc case.

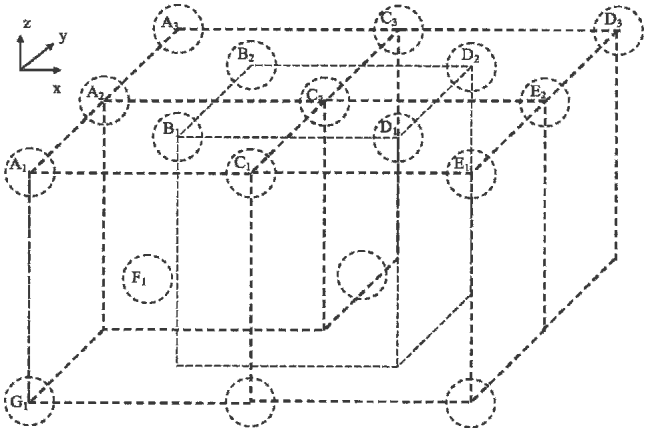

Fig. 9. Sketch of four undistorted fcc cells.

However, the equilibrium equations are much more involved. The sphere A_1 in the top layer interacts with eight neighboring spheres (four in the top layer and four in the middle layer) plus the top wall. Likewise, the sphere G_1 interacts with eight neighboring spheres plus the bottom wall. The sphere F_1 in the middle layer interacts with twelve neighboring spheres, four in the (x, y) plane and in equal separation distances, four in the (x, z) plane, but not in equal separation distances, and four not exactly in the (y, z) plane due to the misalignment of the three layers of spheres. It is conceivable that solving the ten equations would be more difficult than the bcc case and require even more careful selections of the initial values.

It is expected that the results of computation would be similar to those of the rc and bcc cases, and the qualitative features of the flow configuration would remain the same.

SUMMARY AND DISCUSSION

This work is concerned with the effect of settlement on the flow behavior of a dense slurry. At first the transient flow of one layer of spheres embedded in a carrier liquid is studied. It is found that, under the condition of underfill flow, the transient period is very short, and the essential flow behavior may be studied without considering the inertial effect. Gravity causes the spheres to settle but does not terminate the particulate motion by depositing them on the bottom wall. What happens is that, as the spheres settle toward the bottom wall, the stronger wall drag causes them to rotate, which further strengthens the normal separating force between the spheres and the wall. This strengthened separation force counterbalances gravity and keeps the spheres from touching the wall.

The equilibrium configurations of the spheres for three representative packing patterns are then studied. It is found that the spheres can arrange themselves in specific relative positions and different rotation speeds, while all moving with the same translational velocity, so that the forces and moments on each sphere are balanced. The equilibrium configurations deviate from their original undistorted patterns. In the case of the rc packing pattern, the top layer shifts about one radius in the flow direction relative to the bottom layer. In the

case of the bcc packing pattern, the deviation is very small. The distances of the configurations from the bottom wall (h_b) are of course smaller than those from the top wall (h_t), as a result of the gravity effect. However, the h_b values are still much larger than the interparticle distances. This is because, in addition to the rotation effect previously mentioned, the reduced radius of particle-wall interaction is twice as much as that of particle-particle interactions, and a larger reduced radius enhances both the entrainment and squeeze actions.

In the case of neutrally buoyant particles, the stronger particle-wall interactions are not counterbalanced by the weight of the particles. As a result, the particles cluster in the middle of the channel, which makes it reasonable to simulate the slurry flow with the slug flow model.[1]

In the study of dense slurry flows, a diffusion of particles was observed, which appeared to be related to shear rate.[4,5] The observed migration of particles is generally from the higher shear rate region (usually near the wall) to the lower shear rate region (the center of the channel).[6,7] The phenomenon has been modeled as a diffusion process driven by the concentration gradients, with phenomenological coefficients of diffusion depending on the shear rate.[8,9] From the point of view of particle interactions, the spacing between neighboring particles is smaller in the higher concentration region, which produces larger normal separating forces. If on top of the tight spacing a shear gradient is superimposed, particle rotation would be induced, which would further strengthen the normal separating forces. Thus, lubrication mechanisms (entrainment and squeeze actions) offer a plausible kinetic-theoretical explanation for the observed shear-induced migration. The main finding of the current study—that gravity does not terminate the particulate motion by depositing them on the bottom wall; instead the particles are kept away from the wall by the strengthened separation forces—is consistent with the idea of "migration of particles." Guo et al.[10] implemented the particles diffusion idea in their calculation of underfill flows and found better agreement with the measured data than without considering particles diffusion. Their work might be taken as an indirect support to our analysis.

EXPERIMENTAL VERIFICATION

In Ref. 1, an experiment of flowing dense slurries in horizontal channels is described. Two kinds of slurries were prepared. One consisted of glycerine (of density 1261 kg/m^3) as liquid carrier and polymethylmethacrylate (PMMA) spheres (of density 1190 kg/m^3) as fillers. This kind of slurry was used to approximate the situation of neutrally buoyant particles. The measured effective viscosity values for different channel heights are presented in Ref. 1. The other consisted of honey (of density 1340–1400 kg/m^3) as liquid carrier and glass beads (of density 2550 kg/m^3) as fillers. This latter kind of slurry was used to investigate the effect of heavier filler particles. The channel height was controlled to be ten particle diameters. The flows were driven by controlled constant pressure heads. The effective viscosity values, obtained in the same way as in Ref. 1 are presented in Table III (Test 1 and Test 2). For comparison purpose, the case in which PMMA particles with glycerine are used is included in Table III as Test 3, and the theoretical values (available only for neutrally buoyant particles) are given in Table IV. The results are consistent with the common observation that the effective viscosity of a slurry was larger with a higher volume fraction. No settlement of particles onto the bottom wall was observed during these flow tests in spite of the fact that glass beads were markedly heavier than honey. The experiment appears directly supportive to the theoretical finding of this study.

Table III. Measured Values (L/R = 20)

Test	Test Description*	ϕ	Head (mm)	Flow time (min)	μ_{eff}/μ
1	glass beads (s.g. = 2.55, dia. = 200 μm) in honey (s.g. = 1.40, μ = 5.07 Pa s)	0.29	60	15	35.5
2	glass beads (s.g. = 2.55, dia. = 200 μm) in honey (s.g. = 1.34, μ = 5.07 Pa s)	0.61	61	15	40.1
3	PMMA spheres (s.g. = 1.19, dia. = 300 μm) in glycerine (s.g. = 1.261, μ = 1.41 Pa s)	0.49	51	5	37.1

*s.g. = specific gravity; dia. = diameter.

Table IV. Theoretical Values (L/R = 20)

	rc	bcc	fcc
$h_0/R = 0.001$	31.7	26.1	31.3
$h_0/R = 0.01$	21.1	17.3	20.7

It should be noted that the mechanism that prevents the settlement of heavy particles on the bottom wall arises from the strong particle-wall interaction, which is an essential feature of slug flow. Such a mechanism may not exist if slug flow is not achieved. In such a case, one should not expect the effective viscosity to increase with channel height, as demonstrated in Ref. 1.

ACKNOWLEDGEMENTS

This research was partially supported by U.S. Navy Naval Surface Warfare Center under Grant No. 240-6568A. The research was also funded by the Integrated Electronics Engineering Center at the State University of New York at Binghamton. The IEEC receives funding from the New York State Science and Technology Foundation, the National Science Foundation, and a consortium of industrial members.

REFERENCES

1. R. Yang, D.C. Sun, and S. Park, *J. Electron. Mater*. 35, 2016 (2006).
2. MATHCAD 6.0 User's Guide, Mathsoft Inc., Needham, MA.
3. R. Yang, (M.S. Thesis, State University of New York at Binghamton, 1998).
4. D. Leighton and A. Acrivos, *J. Fluid Mech.* 177, 109 (1987).
5. D. Leighton and A. Acrivos, *J. Fluid Mech.* 181, 415 (1987).
6. A. Averbakh, A. Shauly, A. Nir, and R. Semiat, *Int. J. Multiphase Flow* 23, 409 (1997).
7. A. Shauly, A. Averbakh, A. Nir, and R. Semiat, *Int. J. Multiphase Flow* 23, 613 (1997).
8. D. Leighton and A. Acrivos, *Chem. Eng. Sci.* 41, 1377 (1986).
9. R.J. Phillips, R.C. Armstrong, R.A. Brown, A.L. Graham, and J.R. Abbott, *Phys. Fluids A* 4, 30 (1992).
10. Y. Guo, G.L. Lehmann, T. Driscoll, and E.J. Cotts, *1999 Electronic Components and Technology Conference,* (Piscataway, NJ: IEEE, 1999), pp. 71–76.

SYMBOLS

Symbols topped with bars are dimensionless. Most normalized variables are defined in Eqs. (14).

b, d distances defined in Fig. 4; these variables are normalized by R

b_1, b_2, d_1, d_2 distances defined in Fig. 7; these variables are normalized by R

e size of a bcc cell in the (x, y) plane, given in Eq. 18

F friction force

F_{pres} hydrostatic force due to pressure gradient

g gravity constant

h_b clearance from the bottom wall

h_t clearance from the top wall

I moment of inertia of a sphere

L channel height

m mass of a sphere

$\bar{m}$ inertia parameter defined in Transient Motion

n number of cells contained in channel height

p pressure

R particle radius

R_e reduced radius, defined in Eq. 4 of Ref. 1

s smallest clearance between two closest neighboring spheres

t time

U entrainment velocity, defined in Eq. 23 of Ref. 1

(u, w) velocities of sphere in (x, z) directions

W normal separating force

(x, y, z) coordinate system

(x_p, z_p) coordinates of the center of a sphere

$\bar{\alpha}$ density ratio; $= \rho_s/\rho_l$

$\bar{\beta}$ gravity parameter defined in Transient Motion section

$\bar{\delta}$ particle-wall clearance parameter, separately defined in Eqs. (1), (16), and (20)

$\bar{\varepsilon}$ tightness parameter; = s/R

μ viscosity of liquid carrier

ρ_l density of liquid carrier

ρ_s density of filler particles

σ surface tension of liquid carrier

Ω rotation speed of sphere

Subscripts

s due to squeeze action

b at bottom

t at top

l at left

r at right

u between top and middle layers

d between middle and lower layers

g between spheres not lined-up

1,2,3 designating different spheres